Since January 2020 Elsevier has created a COVID-19 resource centre with free information in English and Mandarin on the novel coronavirus COVID-19. The COVID-19 resource centre is hosted on Elsevier Connect, the company's public news and information website.

Inorganica Chimica Acta 517 (2021) 120186

Contents lists available at ScienceDirect

Inorganica Chimica Acta

journal homepage: www.elsevier.com/locate/ica

Research paper

Oxovanadium(IV) and Nickel(II) complexes obtained from 2,2′-dihydroxybenzophenone-S-methyl-thiosemicarbazone: Synthesis, characterization, electrochemistry, and antioxidant capability

Berat İlhan-Ceylan

Department of Chemistry, Faculty of Engineering, Istanbul University-Cerrahpasa, 34320, Avcılar, Istanbul, Turkey

ARTICLE INFO

Keywords:
Oxovanadium(IV)
Nickel(II)
Thiosemicarbazone
X-ray crystallography
Cyclic voltammetry
Antioxidant capability
π-π Stacking interactions

ABSTRACT

2,2′-Dihydroxybenzophenone-S-methyl-thiosemicarbazone and 3-methoxy-salicylaldehyde were reacted in the presence of oxovanadium(IV) or nickel(II) ions to yield the N_2O_2-type-chelate complex. The synthesized complexes were characterized by employing elemental analysis, electronic and infrared spectra, ^{1}H NMR spectra, magnetic measurements, and thermogravimetric analyses. The expected structures of oxovanadium(IV) and nickel(II) complexes were confirmed by using the single-crystal X-ray diffraction method. The presence of π-π stacked dimeric structures provided stronger crystalline formations. The optimized geometries and vibrational frequencies of the compounds were obtained using the DFT/ωB97XD method with the 6-31G (d,p) basis set and compared with the experimental data. The electrochemical characterization of the oxovanadium(IV) and nickel (II) complexes were carried out by using the cyclic voltammetry (CV) method. The oxovanadium(IV) complex gives a ligand-centered oxidation and a metal-centered one electron reduction and oxidation peaks corresponding to the $V^{IV/III}O$ and $V^{IV/V}O$, respectively. The nickel(II) complex gives a ligand-centered oxidation and metal-centered ($Ni^{II/I}$) reduction peaks in a dimethyl sulfoxide (DMSO) solution. The redox potentials were calculated in terms of Gibbs free energy change of the redox reaction at the theory level of M06-L/LANL2DZ/PCM. In addition, the energy gap, HOMO and LUMO distributions were calculated. The total antioxidant capacities of the compounds were determined by using cupric reducing antioxidant capacity (CUPRAC) method, in which the oxovanadium(IV) complex was found to be powerful as an antioxidant agent.

1. Introduction

Vanadium compounds attract great interest owing to their biological importance, use in catalysis, and their rather recent use in alternative electrochemical energy storage technologies like batteries [1–6]. Also, vanadium is an essential bio-element; different from transition elements Mo, Mn, Fe, Co, Cu and Zn, all of which are essential in all life forms, functional vanadium compounds are found only in the form of vanadium nitrogenases and vanadate-dependent haloperoxidases in organisms with a restricted number [7].

Vanadium compounds and their complexes have been employed in the treatment of viral infections such as tuberculosis, human immunodeficiency virus (HIV), and severe acute respiratory syndrome (SARS) [8–12]. There is also an increasing trend over the treatment of diabetes with vanadyl compounds [13]. Some vanadyl complexes were found to be superior to vanadyl sulfate at the physiological pH in terms of significant insulin-mimetic activity [14–15].

The Nickel complexes exhibit a wide range of biological properties such as DNA-binding, protein binding, anticonvulsant, antiepileptic, antifungal, antibacterial, anticancer, antiproliferative, antioxidant and antimicrobial activities [16–18].

There are significant reports on biological studies of oxovanadium and nickel complexes of thiosemicarbazones, such as DNA-binding properties, antiproliferative activities, apoptotic mechanisms on HL60 leukemia cells, antidiabetic properties, and antioxidant properties [19–24].

It is common knowledge that the absence of strong hydrogen-bond donors and acceptors causes aromatic compounds to have a tendency to self-assemble via π-π interactions, and/or C-π interactions. These interactions cause the structure to gain stabilization and can be acquired from X-ray crystal determination [25].

The oxovanadium(IV) (2) and nickel(II) complexes(3) were synthesized from the starting ligand 2,2′-hydroxybenzophenone-S-methyl-thiosemicarbazone (1) and 3-methoxy-salicylaldehyde. Experimental and

E-mail address: beril@istanbul.edu.tr.

https://doi.org/10.1016/j.ica.2020.120186
Received 15 July 2020; Received in revised form 2 December 2020; Accepted 2 December 2020
Available online 9 December 2020

theoretical methods were employed to elucidate the N_2O_2-type chelate complexes (Fig. 1). For compounds 2 and 3, single crystals have been grown, and for further confirmation, analytical and spectroscopic methods have been utilized. The theoretical characterization was accomplished by using the DFT method ωB97XD functional along with a 6-31G (d,p) basis set. The experimental and theoretical data were compared. The newly prepared compounds were subjected to antioxidant capacity studies and cyclic voltammetry (CV) method. The present study aims to investigate biological activity of the synthesized and characterized new template compounds by determining their antioxidant activities.

2. Experimental

2.1. General remarks

All reagent-grade chemicals were commercially purchased and used without further purification. Thermo Finnigan Flash EA 1112 elemental analyzer was used for obtaining the analytical data and a Therma conductivity meter was used for molar conductivities. The fourier transform infrared spectra were recorded on an Agilent Cary 630 ATR spectrometer within 4000–600 cm^{-1}. The electronic spectra were used a Shimadzu UV-2600 UV–visible spectrophotometer, The thermal degradation experiments were carried out on a Shimadzu TGA-50 thermogravimetric analyzer. A constant heating rate of 10 K min^{-1} between room temperature and 900 °C was used. The air flow rate was 50 mL min^{-1} for thermo-oxidative degradation runs. A Bruker Avance-500 model NMR spectrometer in DMSO-d_6 was also used for recording the ^1H NMR spectra. The APCI-MS analyses were carried out in positive and negative ion modes using a Thermo Finnigan LCQ Advantage MAX LC/MS/MS.

Data collection for X-ray crystallography was completed using a Bruker APEX2 CCD diffractometer and data reduction was performed using Bruker SAINT [26]. SHELXT 2018/2 and SHELXL-2018/3 programs were used to solve and refine the structures [27–28]. The structures were solved by direct methods and refined on F^2 using all the reflections. The Gaussian 09 W software package was used for quantum chemical calculations [29]. DFT/ωB97XD and 6-31G (d,p) basis set were employed for the optimized geometry and vibrational wavenumbers. By using the crystallographic data, the initial structures were constructed using the mentioned molecules.

Cyclic voltammograms were recorded using an Ivium Vertex potentiostat/galvanostat system. A Shimadzu UV-2600 UV–vis spectrophotometer along with a pair of matched quartz cuvettes of 1 cm path length were also used for antioxidant capacity measurements. All the determinations were performed at room temperature.

2.2. Synthesis

2,2′-dihydroxybenzophenone-S-methyl-thiosemicarbazone (1) was prepared with slight modifications of the literature method. In the S-alkylation part of synthesis, the compound was stirred in ethanol for a couple of hours to avoid sticky products before applying 5% $NaHCO_3$ and to increase the overall yield [30].

For the synthesis of the template compounds, 1 mmol $VOSO_4{\cdot}5H_2O$ was dissolved in 5 mL of ethanol using an ultrasonic bath at room temperature. 1 mL of triethyl orthoformate was added and the mixture was left at room temperature overnight. The solution was added to a mixture of 2,2′-dihydroxybenzophenone-S-methyl-thiosemicarbazone (1) (1 mmol) and 3-methoxy-salicylaldehyde (1 mmol) in 5 mL of ethanol. For obtaining the convenient product in template condensation, the reaction mixture was kept at room temperature in a dark place without stirring. The mixture was left at room temperature for 3–4 days, and the obtained black product (2) was filtered and washed several times with cold ethanol. The same method for the preparation of nickel (II) template complex (3) was used [31]. The experimental data of the template complexes are as follow:

(2) : Black, m.p. ˃ 370 °C, yield 20%. Molar Conductivity (DMSO, $\Omega^{-1}cm^2mol^{-1}$): 7.1 Anal. Calc. for $C_{23}H_{21}N_3O_6SV$ (518.43 g/mol): C, 53.28; H, 4.08; N, 8.11; S, 6.19. Found: C, 53.01; H, 4.21; N, 7.71; S, 6.43%. UV–Vis ($CHCl_3$) [λ_{max} (nm), log ε ($dm^3\ cm^{-1}\ mol^{-1}$)]: 239(4.79) 266(4.70) 338(4.71) 361(4.71) 440(4.36). IR (cm^{-1}): υ(OH) 3430; υ(C = N^1) 1601; υ(C = N^2) 1582; υ(C_{ar}–O) 1154, 1104; υ(V = O) 970, υ(C—S) 749. MS *m/z* (%):[(M−H_2O) + Na]$^+$ 523.1 (100), [(2 M−2H_2O) + Na]$^+$ 1022.8 (31.35)

(3): Red, m.p. ˃ 370 °C, yield 22%. Molar Conductivity (DMSO, $\Omega^{-1}cm^2mol^{-1}$): 17.1 Anal. Calc. for $C_{25}H_{27}N_3NiO_6S$ (556.26 g/mol): C, 53.98; H, 4.89; N, 7.55; S, 5.76. Found: C, 54.18; H, 4.72; N, 7.76; S, 5.93%. UV–Vis ($CHCl_3$) [λ_{max} (nm), log ε ($dm^3\ cm^{-1}\ mol^{-1}$)]: 219 (4.50) 226 (4.53) 240 (4.78) 315 (4.44) 403 (4.38) 503 (3.84) 579 (3.74). IR (cm^{-1}): υ(OH) 3345; υ(C = N^1) 1612; υ(C=N^2) 1585; υ(C_{ar}–O) 1151, 1128; υ(C—S) 745. MS *m/z* (%): [2 M + Na]$^+$ 1006.8 (100), [M + Na]$^+$ 514.2 (46.15). ^1H NMR (DMSO-d_6, 30 °C, δ ppm): 9.71 (s, 1H, OH), 8.20 (s, 1H, N^4 = CH), 7.31(td, J = 7.32, 7.80, 2H, d, e), 7.27 (td, J = 7.57, 7.81, 1H, g), 7.04 (dd, *J* = 7.57, 1.70, 1H, i), 6.98 (t, J = 8.78, 8.78, 3H, c, f, j), 6.93 (dd, J = 6.35, 1H, a), 6.91 (t, J = 7.32, 7.80, 1H, h), 6.64 (t, *J* = 8.30, 7.81, 1H, b), 6.54 (td, *J* = 7.57, 7.57, 1H, k), 4.35 (t, *J* = 5.1 Hz, 1H, **HO**-CH_2-CH_3) 3.78 (s, 3H, O-CH_3), 3.44 (m, 2H, HO-**CH_2**-CH_3), 2.23 (s, 3H, S-CH_3), 1.05 (t, *J* = 6.83, 7.32 Hz, 3H, HO-CH_2-**CH_3**).

2.3. Cyclic Voltammetry

Electrochemical measurements were performed with a conventional three electrode cell. The Glassy carbon electrode (GCE) with a 3.0 mm diameter was used as the working electrode. The circuit was completed with a saturated Ag/AgCl and a platinum wire, which served as the reference and counter electrode, respectively. The GCE used as a working electrode was polished with alumina slurry (Buehler Micropolish) using a polishing pad (Buehler-102 mm) and washed with water before each experiment. Measurements were performed in 1 × 10^{-3} M

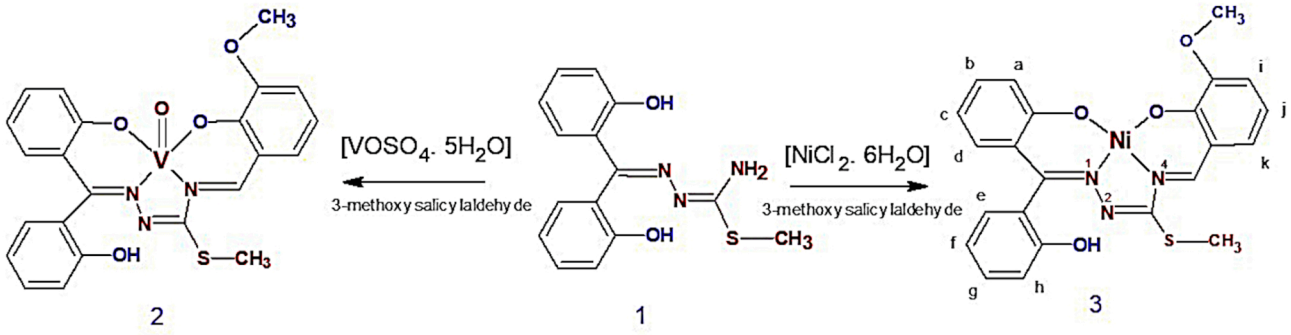

Fig. 1. Synthesis scheme of oxovanadium(IV) (**2**) and nickel(II) (**3**) complexes.

oxovanadium(IV) (2) and nickel(II) (3) complexes solutions in dimethyl sulfoxide containing 0.1 M of tetrabutylammonium perchlorate (TBAP) supporting electrolyte under a nitrogen atmosphere.

2.4. Antioxidant capacity

The CUPRAC method was employed to assess the total antioxidant capacity of the compounds [32]. Antioxidant activity deals with reaction kinetics and the rate of chemical oxidation of the antioxidant in question or the rate of quenching of the reactive species by the antioxidant [33]. Under the same conditions, molar absorption coefficients were calculated for all of the compounds. Trolox equivalent antioxidant capacity (TEAC) coefficients were calculated as a fraction of the molar absorptivity of the selected compound to that of Trolox. 1 mL 10 mM $CuCl_2{\cdot}2H_2O$, 1 mL 7.5 mM neocuproine (Nc), 1 mL 1.0 M pH 7 NH_4OAc buffer, x mL antioxidant sample solution, and (1.1- x) mL H_2O were put, in this order, to a test tube. The total volume of this mixture is 4.1 mL, and this was incubated for half an hour, and the absorbance was recorded against a blank solution of reagents at 450 nm. The TEAC coefficients were found by dividing the molar absorptivity of each compound by the trolox molar absorptivity, which is 1.67×10^4 L mol^{-1} cm^{-1}. Trolox and ascorbic acid were used as standards.

3. Result and discussion

3.1. Synthesis

2,2′-Dihydroxybenzophenone reacts with thiosemicarbazide with only N(1) hydrazine nitrogen, while N(4) atom does not give such a reaction. However, N(4) atom can give the template synthesis reaction. Thus, template condensation could be used to prepare complexes of the ligands which could not be obtained with a simple condensation. These reactions mainly work with the directing effect of the metal ion and this function of the metal ion is coined as “template effect” [34].

2,2′-dihydroxybenzophenone-S-methyl-thiosemicarbazone (1) was condensed with 3-methoxy-salicylaldehyde in the presence of the template effect of oxovanadium(IV) or nickel(II) ions. The template reaction leads to the formation of complexes 2 and 3, in which the L behaved as a dibasic thiosemicarbazidato ligand (Fig. 1). The complexes are soluble in ethanol and chloroform, and extremely soluble in dimethyl sulfoxide and N,N dimethylformamide.

3.2. Molar Conductivity Measurements

The molar conductivities of S-methyl-thiosemicarbazone (1), oxovanadium(IV) complex (2) and nickel(II) complex (3) were measured in 10^{-3} M DMSO solution at room temperature with the obtained results of 0.7, 7.1 and 17.1 $\Omega^{-1}cm^2mol^{-1}$, respectively. The low molar conductivity values reveal the non-electrolytic nature of the metal complexes. The structures are non electrolytic and no anions are present outside the coordination sphere [35–37].

3.3. Crystallography

The molecular views of the oxovanadium(IV) complex (2) and nickel (II) complex (3) were shown in Figs. 2 and 3 and Table 1 summarizes the principal crystalline data and structural refinement parameters.

Oxovanadium(IV) complex (2) and nickel(II) complex (3) were crystallized in the monoclinic space group $P2_1/n$ (2) and $P2_1/c$ (3) with Z = 4. Tables 2-3 and Tables S1a/b -S4a/b present the bond lengths, bond angles, torsion angles, atomic coordinates, and hydrogen bonds for 2 and 3.

The optimized structures of complexes 2 and 3 are square-pyramidal and square-planar, respectively. The resulted structures are in a good agreement with the results of X-ray analyses. Some selected optimized and values of bond lengths and angles are shown in Table 2. In the

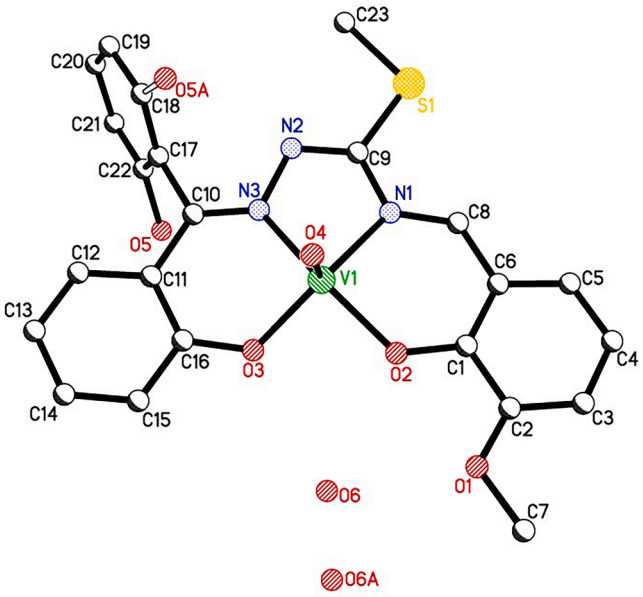

Fig. 2. Perspective view of oxovanadium(IV) complex (**2**) with atomic numbering.

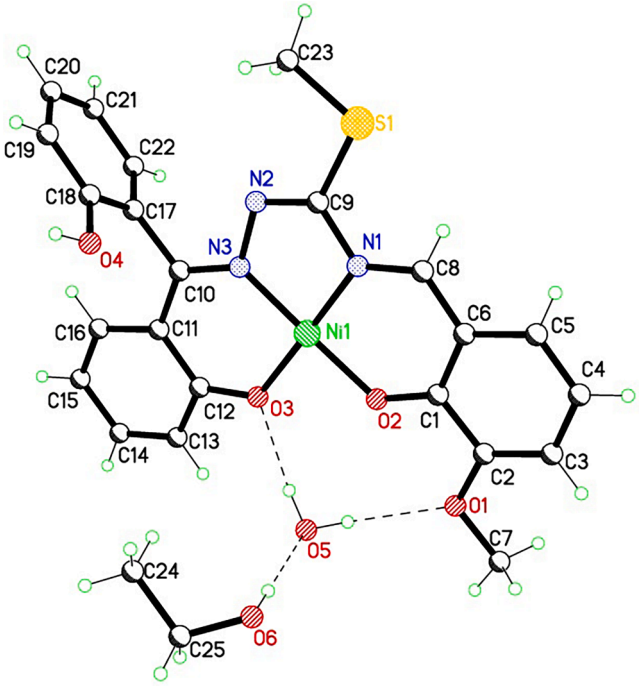

Fig. 3. Structure of nickel (II) complex (**3**) with atom numbering. Hydrogen bonds are shown as dashed lines.

optimized V = O bonds, the V1-O4 (double bond character) with a bond length of 1.589 Å (experimental) and 1.601 Å (theoretical) [38].

The non-coordinated phenolic oxygen atom is disordered over two positions (O5-C22 and O5A- C18) with site occupancies of 0.72 and 0.28 in the oxovanadium (IV) complex (2), respectively. Moreover, the asymmetric unit contains a water molecule which is disordered (O6 and O6A), and this was modeled over two positions site occupancies of 0.604 and 0.396, respectively. (Fig. 2) The $OH_{water}\cdots O$ hydrogen bonds form a 2D hydrogen bond network in oxovanadium(IV) complex (2) in the Fig. 4.

The smallest bond angle of complex 2 is N(3)-V(1)-N(1), a five-

Table 1
Crystalline data and refinement parameters of **2** and **3**.

Compound	Oxovanadium (IV) complex (2)	Nickel (II) complex (3)
CCDC number	1988906	2013189
Chemical formula	C_{23} H_{21} N_3 O_6 S V	C_{25} H_{27} N_3 Ni O_6 S
Crystal size (mm^3)	0.17 × 0.12 × 0.09	0.14 × 0.11 × 0.08
Formula weight (g/mol)	518.43	556.26
Temperature (K)	293(2)	293(2)
Wavelength (Å)	0.71073	0.71073
Crystal system	Monoclinic	Monoclinic
Space group	$P2_1/n$	$P2_1/c$
Unit cell parameters		
a, b, c (Å)	9.3252(6), 16.5156(13), 17.4414(12)	11.7325(6), 12.2110(6), 17.8101(8)
γ, β, γ	90°, 97.551(6)°, 90°	90°, 93.079(5)°, 90°
Cell volume ($Å^3$)	2662.9(3)	2547.9(2)
Z	4	4
Density (g/cm^3)	1.293	1.450
Abs. coefficient (mm^{-1})	0.490	0.889
F_{000}	1068	1160
Index ranges	$-11\leq h\leq 12$, $-21\leq k\leq 11$, $-22\leq l\leq 11$	$-8\leq h\leq 15$, $-16\leq k\leq 14$, $-22\leq l\leq 19$
Reflections collected	9152	11,586
Independent reflections	5256	5831
R_{int}	0.0485	0.0382
Data/ restraints / parameters	5256 / 0 / 330	5831 / 0 / 333
Goodness of fit on F^2	0.997	1.022
Final R indices [$I > 2\sigma$ (I)]	R1 = 0.0813, w$R2$ = 0.2182	R1 = 0.0574, wR2 = 0.1269
	R1 = 0.1777, w$R2$ = 0.2796	R1 = 0.1251, wR2 = 0.1715
Δρmax , Δρmin ($e/Å^3$)	0.779, −0.310	0.585, −0.390

membered ring with 75.27° experimentally, whose theoretical counterpart is 77.24°. O(3)-V(1)-N(3) bond angle in the six-membered ring is 86.65° (experimental) while it is 85.07° (theoretical). Another six-membered ring is formed with O(2)-V(1)-N(1), and its experimental bond angle is 87.93°, whereas it is 85.65° (theoretical) and it is harmonious with the other six-membered ring system. Bond lengths of oxovanadium ion with nitrogens are approximately 0.1 Å longer than the bonds formed with oxygens.

The Addison tau parameter [39] was calculated, which gives the numerical value of the complex as how similar the structure to ideal square pyramidal and trigonal bipyramidal geometries, as $\tau = 0.156$ by plugging O(2)-V(1)-N(3) as β (148.68°) and O(3)-V(1)-N(1) as α (139.32°) (Table 2) in the oxovanadium(IV) complex (2). The ideal square pyramidal geometry is represented by $\tau = 0$, and our result is very close to this value.

With the template effect of nickel(II) ion, S-methyl-thiosemicarbazone (1) forms an ONNO square-planar geometry with the Ni (II) ion at the center, forming the Ni complex (3). The square planar geometry in the Ni(II) complex (3) is formed by the phenolic oxygen (O3), thiosemicarbazone imine nitrogen (N2), terminal nitrogen (N3), and 3-methoxy-salicylaldehyde oxygen (O2).

Asymmetric unit contains a complex molecule, a water and an ethanol molecule in the nickel(II) complex (3) (Fig. 3). There are hydrogen bondings and significant intermolecular interactions in the nickel(II) complex (3) (Fig. 5).

The multiplicity of substituents bound to the aromatic rings and sulfur atom in thiosemicarbazones is an important factor in the outcome of different chemical properties [40]. The methoxy and hydroxy groups in the nickel(II) complex (3) structure attend the hydrogen bond. Each water molecule (O5) involves in four hydrogen bondings (two as donor with methoxy (O1) and phenolate oxygen atoms (O3) and two as acceptors with phenolic (O4) and alcoholic atoms (O4). The bond lengths

Table 2
Bond lengths [Å] and angles [°] for **2** and **3**. (Symmetry transformations used to generate equivalent atoms).

	Experimental	Calculated		Experimental	Calculated
2					
V(1)-O(4)	1.589(4)	1.601	O(2)-V(1)-N(3)	148.68(18)	147.25
V(1)-O(3)	1.894(5)	1.902	O(4)-V(1)-N(1)	108.9(2)	106.7
V(1)-O(2)	1.942(4)	1.945	O(3)-V(1)-N(1)	139.32(18)	140.16
V(1)-N(3)	2.042(5)	2.063	O(2)-V(1)-N(1)	87.93(18)	85.65
V(1)-N(1)	2.047(5)	2.075	N(3)-V(1)-N(1)	75.27(18)	77.24
O(4)-V(1)-O(3)	110.6(2)	112.0	C(1)-O(2)-V(1)	129.9(4)	133.1
O(4)-V(1)-O(2)	107.6(2)	108.2	C(16)-O(3)-V(1)	125.7(4)	130.6
O(3)-V(1)-O(2)	89.5(2)	90.8	C(8)-N(1)-V(1)	126.5(4)	126.6
O(4)-V(1)-N(3)	102.9(2)	103.5	C(9)-N(1)-V(1)	112.6(4)	110.9
O(3)-V(1)-N(3)	86.65(18)	85.07	C(10)-N(3)-V(1)	129.0(4)	129.4
3					
Ni(1)-O(3)	1.832(3)	1.854	C(1)-O(2)-Ni(1)	127.2(3)	129.052
Ni(1)-N(1)	1.836(3)	1.885	C(12)-O(3)-Ni(1)	126.6(2)	128.091
Ni(1)-N(3)	1.840(3)	1.871	C(18)-O(4)-H(4)	109.5	112.706
Ni(1)-O(2)	1.850(2)	1.865	C(8)-N(1)-C(9)	121.9(4)	123.315
O(3)-Ni(1)-N(1)	178.85(13)	178.572	C(8)-N(1)-Ni(1)	127.7(3)	126.906
O(3)-Ni(1)-N(3)	94.85(13)	93.846	C(9)-N(1)-Ni(1)	110.4(3)	109.779
N(1)-Ni(1)-N(3)	84.16(13)	84.726	C(9)-N(2)-N(3)	110.8(3)	111.784
O(3)-Ni(1)-O(2)	86.40(11)	87.944	C(10)-N(3)-N(2)	115.5(3)	116.161
N(1)-Ni(1)-O(2)	94.59(13)	93.483	C(10)-N(3)-Ni(1)	129.3(3)	129.811
N(3)-Ni(1)-O(2)	178.73(13)	178.187	N(2)-N(3)-Ni(1)	115.2(2)	114.027

Table 3
Hydrogen bonds for **2** and **3** [Å and °]

D-H…A	d(D-H)	d(H…A)	d(D…A)	<(DHA)
2				
O(5a)-H(5a)…O(6a)#1	0.82	2.03	2.715(15)	141.4
O(6a)-H(6Ba)…O(2)	0.85	2.40	3.027(12)	130.6
O(6a)-H(6Ba)…O(3)	0.85	2.46	3.038(12)	126.3
O(6Ab)-H(6AAb)…O(4)#2	0.85	2.09	2.861(19)	150.0
3				
O(4)-H(4)…O(5)#1	0.82	1.95	2.754(5)	164.4
O(5)-H(5A)…O(1)	0.85	2.12	2.944(4)	163.9
O(5)-H(5B)…O(3)	0.85	1.97	2.820(4)	174.9
O(6)-H(6)…O(5)	0.82	2.03	2.854(6)	179.5

#1 -x,-y + 1,-z + 1 #2 -x + 1/2,y + 1/2,-z + 1/2

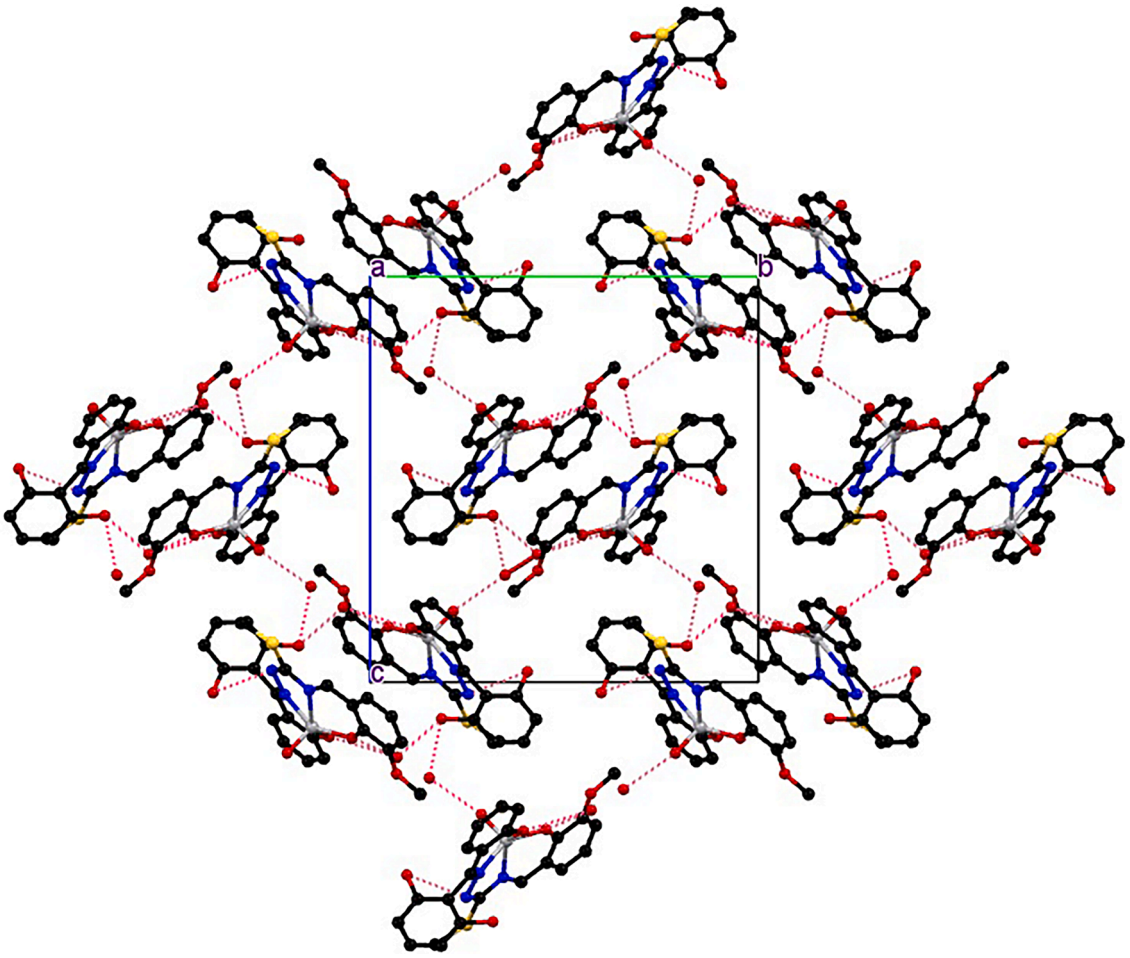

Fig. 4. The $OH_{water}\cdots O$ hydrogen bonds forming a 2D hydrogen bond network in oxovanadium(IV) complex (**2**).

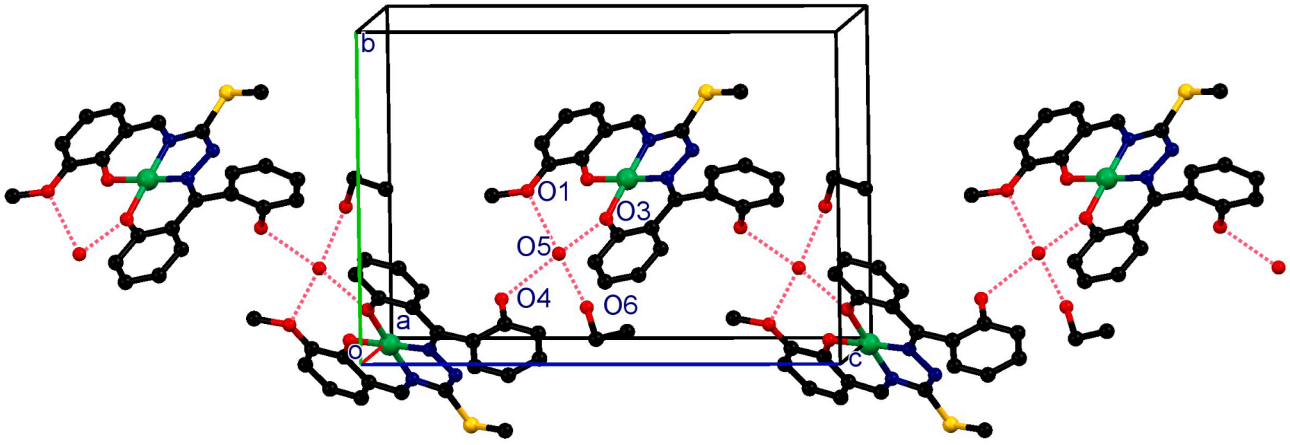

Fig. 5. Hydrogen bond chain in nickel(II) complex (**3**) along the *c* axis. Hydrogen bonds are shown as dashed lines.

formed are between O1-O5 (2.944 Å), O3-O5 (2.820 Å), O4-O5 (2.754 Å) and O6-O5 (2.854 Å), they are very close to each other as given in Table 3.

In the nickel(II) complex (3), the smallest bond angle is N(1)-Ni(1)-N (3), a five-membered ring, yielded an experimental value of 84.16°, while it is 84.726° theoretically. The bond angle of the six-membered ring of O(3)-Ni(1)-N(3) is 94.85° (experimental), while it is 93.846° (theoretical). Another six-membered chelate ring is formed with the contribution of N(1)-Ni(1)-O(2), and the bond angle is 94.59° (experimental), whereas it is 93.483° and it is harmonious with the other six-membered chelate ring. The bond lengths of nickel atom with nitrogens and oxygens are very close to each other, which is indicative of the square-planar geometry.

Complex molecules are further linked by π-π stacking interactions. It has been observed that aromatic rings in complex structures are linked in the same parallel plane with the ligand of the other complex molecule by π-π interactions. The π-π stacking interaction value in oxovanadium (IV) complex (2) is 3.292 Å (Fig. S1), whereas the π-π stacking

interaction values in nickel(II) complex (3) are between 3.418 and 3.441 Å (Fig. S2). The molecules have a linkage of π-π stacking, thereby the structure is stabilized. [25,41–42].

3.4. Ultraviolet–visible spectrophotometry

The electronic spectra were recorded by using the chloroform solutions of the compounds in the range of 200 to 900 nm (Fig. S3). In the electronic spectrum of 2,2′-dihydroxybenzophenone-S-methyl-thiosemicarbazone (1), the $\pi \rightarrow \pi^*$ transition was observed at 260 nm due to the presence of benzophenone ring system, whereas this transition was observed at 266 and 240 nm for oxovanadium(IV) complex (2) and nickel(II) complex (3), respectively.

The $n \rightarrow \pi^*$ transition of (1) occurs owing to the presence of azomethine and thioamide moieties, and this transition was observed at 306 nm and 340 nm, respectively. In the oxovanadium(IV) complex (2), these transitions were shifted to 338 and 361 nm, while for nickel(II) complex (3), only one shifted transition at 315 nm was observed [35,43].

For the oxovanadium(IV) complex (2), the LMCT band was observed at 440 nm [44]. The parameters, being the donor groups in the complexes, showed high accuracy for square pyramidal VO complexes; octahedral complexes yielded a significant shift [45].

Another ligand to metal charge transfer band was seen in the nickel (II) complex (3) at 403 nm. The more intense charge transfer bands were observed at 503 nm and 509 nm. The UV peaks for (3) indicated that square planar geometry was attributed to the complex, and a possible $^3T_1 \rightarrow {}^3T_2$ transition is attributed to these peaks [46–47].

3.5. Infrared spectra

The most prominent spectral bands of the starting material 2,2′-dihydroxybenzophenone-S-methyl-thiosemicarbazone (1) in the IR spectrum are ν(2′-OH) at 3453 cm^{-1}, $\nu_{as}(NH_2)$ at 3349 cm^{-1}, $\nu_s(NH_2)$ at 3284 cm^{-1}, ν(2-OH) at 3106 cm^{-1}, $\delta(NH_2)$ at 1630 cm^{-1}, $\nu(C = N^1)$ at 1600 cm^{-1} and $\nu(N^2 = C)$ were recorded at 1561 cm^{-1} [47]. Due to the template reaction, the $\nu_{as}(NH_2)$, $\nu_s(NH_2)$, and ν(2-OH) bands disappeared, and the new $\nu(N^4 = C)$ band has been formed by the condensation reaction of the thiosemicarbazone with salicylaldehyde, which has been observed at 1581 cm^{-1} (2) and 1585 cm^{-1} (3), respectively. The band at 970 cm^{-1} was assigned to υ (V = O) for oxovanadium (IV) complex (2)[48].

3.6. ^1H NMR Spectra

Proton nuclear magnetic resonance data supports the formation of the Ni(II) template complex (Fig. S4). The OH and N^4H peaks disappear upon coordination to the metal ion, forming the ONNO template complex framework. In the investigation of ^1H NMR spectrum of the reaction product between 2,2′-dihydroxybenzophenone-S-methyl-thiosemicarbazone (1) and 3-methoxy-salicylaldehyde in the presence of the metal ion, it was observed that there was a singlet peak at δ 8.20 ppm for the N^4 = CH system, thereby supporting the template structure [49]. There is doublet of doublets, triplets, and triplet of doublets peaks arising for the eleven protons in the aromatic system. The singlet peaks were found for the methoxy and S-methyl groups at δ 3.78 and 2.23 ppm.

3.7. Electrochemistry

The electrochemical behaviors of the complexes were examined with cyclic voltammetry method in the potential range of −1.5 to + 1.5 V vs. Ag/AgCl in TBAP/DMSO electrolyte system (Fig. 6). The complexes which contain different metal ions exhibited excellent voltammetric behavior, including metal and ligand-centered redox processes in DMSO. All electrode processes were characterized by the ratio of the cathodic to anodic peak currents (I_{pa}/I_{pc}) and peak-to-peak separation (ΔE_p). The electrochemical parameters obtained from CV at 0.05 Vs^{-1} scan rate were listed in Table 4.

The CV of oxovanadium(IV) complex (2) in a DMSO solution shows a

Table 4
Electrochemical Parameters of 1.0 × 10^{-3}M oxovanadium(IV) (**2**) and nickel(II) (**3**) complexes in DMSO/TBAP at 0.05 Vs^{-1} scan rate.

Complexes	Redox Process	Peak Parameters [a]$E_{1/2}$(V)	[b]i_{pa}/i_{pc}	[c]ΔE_p (mV)
2	$V^{IV/V}O$	0.53	1.04	60
	$V^{IV/III}O$	−0.83	0.27	80
	L/L^+	1.23	–	–
3	$Ni^{II/I}$	−0.78	0.14	40
	L/L^+	1.22	–	–

[a] $E_{1/2}$ values are given for the reversible and quasi-reversible processes. E_{pc} or E_{pa} values are given for the irreversible processes.
[b] i_{pa} and i_{pc} are the anodic and cathodic peak currents, respectively.
[c] ΔE_p is peak to peak separation ($\Delta E_p = |E_{pa} - E_{pc}|$).

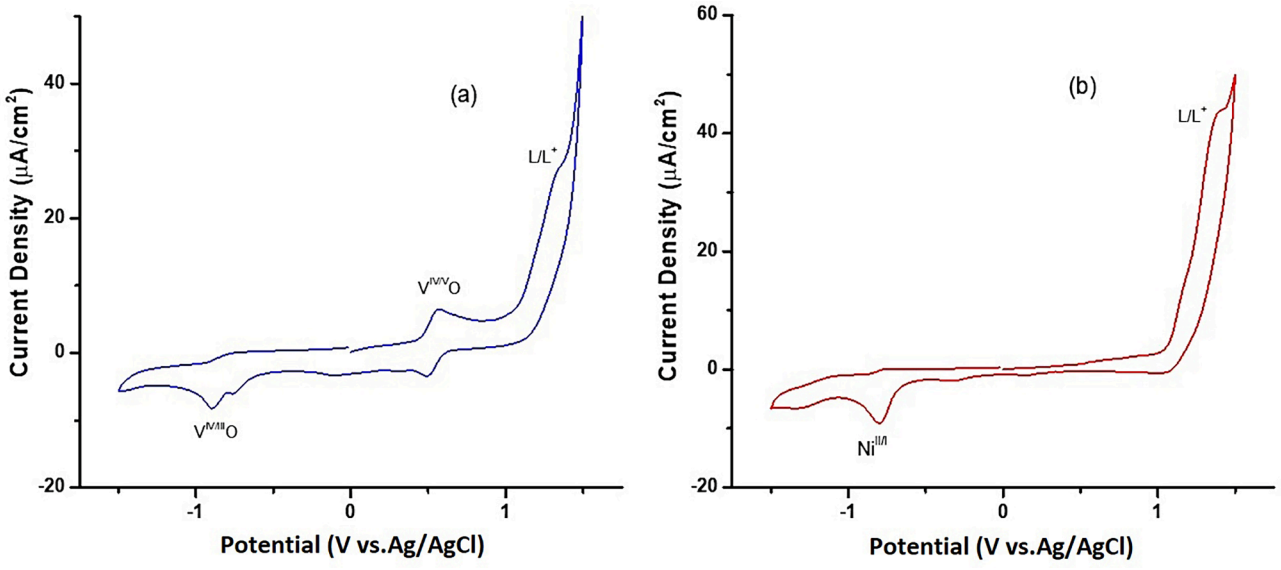

Fig. 6. CVs of oxovanadium(IV) complex (**2**) (a) and nickel(II) complex (**3**) (b) in 0.1 M TBAP/DMSO solution at 0.05 Vs^{-1} scan rate.

reversible redox response at 0.53 V and an irreversible redox response at −0.83 V versus Ag/AgCl reference electrode (Fig. 6a) [35,50–52]. The redox couple observed in the positive side can be assigned to a metal-centered oxidation process corresponding to oxidation of $V^{IV}O$ to $V^{V}O$ at 0.050 Vs^{-1} scan rate. ΔE_p value of the oxidation couple is calculated as 60 mV, and the value of i_{pa}/i_{pc} is about 1, indicating the reversible character of this redox process. The reduction couple shows an irreversible character (ΔE_p about 80 mV and I_{pa}/I_{pc} about 0.27) attributed to the $V^{IV}O$ to $V^{III}O$ reductive response at −0.88 V. Even though ΔE_p value of the reduction couple is in reversible range, very small I_{pa}/I_{pc} value shows the irreversible character of the redox process to the chemical reaction. The presence of the shoulder located at −0.76 V has been reported previously [31]. In this study, this shoulder is attributed to probable adsorption process occurred at the electrode/electrolyte interface. A third oxidation peak observed at more anodic potential (approximately at ~ 1.32 V), is associated with a ligand-based oxidation (L/L^{+}) [47,49].

Similarly, for nickel (II) complex (3), one irreversible oxidative ligand-based response (L/L^{+}) was observed at 1.40 V on the positive side, and one irreversible metal-based ($Ni^{II/I}$) reduction couple appeared at −0.80 V on the negative side of the CV (Fig. 6b) [35,53–54]. The experimental parameters obtained from CV for nickel (II) complex (3) indicate that both oxidation and reduction peaks have an irreversible character at 0.05 Vs^{-1} scan rate (Table 4). For further confirmation of the redox process occurred on electrode/electrolyte interface, the effect of increasing scan rate is investigated for both (2) and (3) complexes (Fig. S5). Considering Fig. S6, with increasing scan rate, new shoulders appear at more positive potentials than that of $Ni^{II/I}$ reduction peaks. These new peaks are attributed to the adsorption process occurred on the electrode surface when applied high scan rates (˃75 mVs^{-1}). For further clarification of this idea, the logarithms of peak currents (log ip) as a function of log ν for oxovanadium(IV) complex (2) and nickel (II) complex (3) were presented in Fig. S6 a and b, respectively. It is well known that the value of the slope is less than 0.5 is explained for diffusion-controlled process, whereas that of higher than 0.5 is indicated the adsorption-controlled process [55]. Therefore, in this study the slope value of complex (2) is obtained as 0.51 indicating the mixed adsorption-diffusion controlled process. As for complex (3), the slope value is calculated as 0.61, showing an adsorption controlled process. These results further support the discussions related to Fig. S6.

The electrochemical behaviors of the complexes were also investigated by density functional theory (DFT). Redox potentials were calculated according to the procedures in the previous publication [49,56–57]. In these calculations, molecular geometries (the ligand, the complex 2 and 3) for both neutral or radical ion (anion and cation) in gas-phase and in solution (DMSO) were calculated by DFT/M06-L with LANL2DZ basis set in conjunction with a polarizable continuum model (PCM). In addition, to verify all the optimized structures are to be local minima, the vibrational wavenumbers were computed analytically. All the calculations are evaluated using GAUSSIAN 09.

The reduction potentials of the ligand, complex 2 and complex 3 against Ag/AgCl was found to be −0.346, −1.688, and −1.472 V, respectively. A low and negative redox potential is indicative of a reducing environment [58]. The oxidation potentials of the ligand, complex 2 and complex 3 against Ag/AgCl were found to be −0.163, 0.009, and −0.442 V, respectively. The low oxidation potential implies that the structure is easier to be oxidized. The antioxidant power of complex 2 is higher than that of complex 3. Experimental data and the theoretical values are seen to be in a good agreement.

The energies and spatial distribution of the LUMO and HOMO orbitals for the neutral, reduction and oxidation states of the ligand, complex 2 and 3 are given in Figs. S7-S9 respectively in supplementary data. For the reduction of complex 2, LUMO shows π electron orbitals located at the phenyl rings.

3.8. Thermogravimetric analysis

The starting material and complexes are stable at room temperature. The TGA spectrum showed that the starting material (1) featured a decomposition with 3 stages (Fig. 7 and Fig S10-S12). Compound 1 lost 25% of the starting weight at 201–206 °C with the elimination of C-(S-CH_3)–NH_2 moiety (Table 5). Between 261 and 383 °C, C_6H_5-OH + OH groups, constituting of 37%, were eliminated, and the last 30% portion was observed between 444 and 621 °C and C_6H_5-C group left the remainder. The complex 2 lost 8% of the initial weight in the range 112–151 °C from CH_3-CH_2-OH + H_2O and a 36% portion between 290 and 360 °C from the elimination of 2-OH-4-CH_3O-C_6H_5-C + S-CH_3 groups. In the 380–440 °C range, a 39% elimination was observed for C_6H_5-C-C_6H_5 moiety. The VO compound remains intact [59–60].

The nickel(II) complex (3) showed the first loss of 12% by the elimination of CH_3-CH_2-OH + H_2O groups. The second loss occurred at 43% within 322–352 °C, from the elimination of 2-OH-4-CH_3-C_6H_5-C + NC–(S-CH_3)-N groups. The third loss was at 7% (416–427 °C) due to 2-(OH) + 2′-(OH). The NiO compound remains intact [61–62].

3.9. Antioxidant efficiency

The antioxidant efficiencies were assayed for 2,2′-dihydroxybenzophenone-S-methyl-thiosemicarbazone (1), its oxovanadium(IV) complex (2), and its nickel(II) complex (3) by using the CUPRAC method against Trolox (TR) being the standard reference compound. Trolox (6-hydroxy-2,5,7,8-tetramethylchroman-2-carboxylic acid) is a synthetic water-soluble analog of α-tocopherol, known as the most active form of vitamin E. The TEAC coefficients of compounds 1–3 and ascorbic acid as a reference, is shown in Table 6. The TEAC coefficients of compounds 1–3 are 1.5, 2.0, and 0.6, respectively.

Associated with an electron donation from the phenolic hydroxyl group, it was deduced that the electron transfer-based antioxidant capacity could be caused by the former. The oxovanadium(IV) complex (2) was found to be a more potent antioxidant than the 2,2′-dihydroxybenzophenone-S-methyl-thiosemicarbazone (1). It is essential to know the antioxidant properties of biologically active compounds for using them in pharmacy and medicine. Free radicals are capable of oxidizing the biomolecules and cause degenerative diseases. Oxidative damage can play a serious role in human diseases like cancer, emphysema, cirrhosis, and diabetes. Antioxidants terminate the attack by the reactive species like free radicals and prevent ageing and different diseases

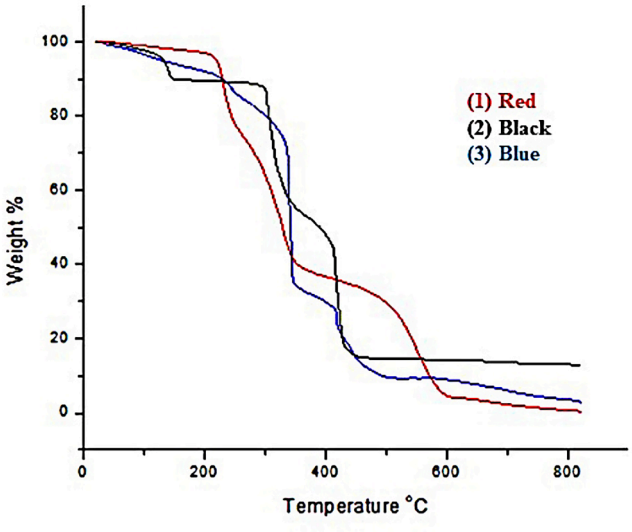

Fig. 7. TGA–DTGA curves of the 2,2′-dihydroxybenzophenone-S-methyl-thiosemicarbazone (**1**) oxovanadium(IV) complex (**2**) and nickel(II) complex (**3**).

Table 5
Thermogravimetric data for **1**, **2** and **3**.

Compound	Step	Temperature Range (°C)	DTG (°C)	Weight loss(%) Found (Calcd.)	Residue
1	1st	201–260	232	25(24.91)	
	2nd	261–383	330	37(36.54)	
	3rd	444–621	546	30(29.90)	
2	1st	112–151	138	8(7.91)	
	2nd	290–360	302	36(35.32)	
	3rd	380–440	414	39(38.20)	VO
3	1st	209–247	235	12(11.51)	
	2nd	322–352	338	43(42.60)	
	3rd	416–427	419	7(6.11)	NiO

Table 6
TEAC coefficient of **1**, **2**, **3** and ascorbic acid.*

Compounds	TEAC
1	1.5 ± 0.01
2	2 ± 0.01
3	0.6 ± 0.01
Ascorbic acid	1.0 ± 0.01

* We expressed the results as the mean ± standard deviation (SD) of triplicate determinations.

linked to oxidative damages in the body. [63–67] The antioxidant activities of naphthaldehyde-based S-alkylthiosemicarbazone oxovanadium(IV) complexes [44] were found to be less than those of benzophenone thiosemicarbazone oxovanadium(IV) complexes. The oxovanadium(IV) complex (2) might be used as an active drug ingredient due to this antioxidant capacity.

Table 6.

4. Conclusion

The new oxovanadium(IV) complex (2) and nickel(II) complex (3) were synthesized and characterized. The structures were confirmed by recording the single crystal X-ray diffraction. The theoretical bond lengths and bond angles were seen to be in excellent accuracy with the experimental ones.

Electrochemical measurements of the oxovanadium(IV) complex (2) show that the complex has irreversible ligand-centered (L/L^+) oxidation and one reversible $V^{IV}O$ to $V^{V}O$ wave on the oxidation side and one irreversible $V^{IV}O$ to $V^{III}O$ wave on the reduction side in the cyclic voltammograms. Nickel(II) complex (3) also displays an irreversible ligand-centered (L/L^+) oxidative response in addition to a metal-centered one-electron Ni^{II}/Ni^{I} reduction couple.

Electrochemical measurements show that oxovanadium(IV) complex (2) has a less positive oxidation potential value indicating that it has a better antioxidant activity compared to nickel(II) complex (3). Thus the electrochemical data confirms the CUPRAC results.

Declaration of Competing Interest

The authors declare that they have no known competing financial interests or personal relationships that could have appeared to influence the work reported in this paper.

Acknowledgements

I dedicate this manuscript to Dr. Bahri ÜLKÜSEVEN and Dr. Yasemin KURT, both of whom directed my career. Dr. Olcay BÖLÜKBAŞI is sincerely thanked for her support of theoretical calculations in Gaussian software.

This work was supported by the Research Fund of Istanbul University-Cerrahpasa. Project No: 24195 and 34846.

Appendix A. Supplementary data

CCDC numbers 1988906 for 2 ($C_{23}H_{21}N_3O_6SV$) and 2013189 for 3 ($C_{25}H_{27}N_3Ni\,O_6S$) contain the supplementary crystallographic data. The data can be obtained, free of charge, via http://www.ccdc.cam.ac.ac.uk/conts/retrieving.html, or from the Cambridge Crystallographic Data Center, 12, Union Road, Cambridge CB2 1EZ, UK; fax: +44 1223 336 033; or email: deposit@ccdc.cam.ac.uk. Supplementary data to this article can be found online at https://doi.org/10.1016/j.ica.2020.120186.

References

[1] J. Pisk, J.C. Daran, R. Poli, D. Agustin, J. Mol. Cat. A: Chem. 403 (2015) 52–63, https://doi.org/10.1016/j.molcata.2015.03.016.
[2] V. Tahmasebi, G. Grivani, G. Bruno, J. Mol. Structure. 1123 (2016) 367–374, https://doi.org/10.1016/j.molstruc.2016.06.038.
[3] H.J. Parker, C.J. Chuck, T. Woodman, M.D. Jones, Catalysis Today. 269 (2016) 40–47, https://doi.org/10.1016/j.cattod.2015.08.045.
[4] S. Barroso, P. Adão, F. Madeira, M.T. Duarte, J.C. Pessoa, A.M. Martins, Inorg. Chem. 49 (2010) 7452–7463, https://doi.org/10.1021/ic1007704.
[5] A. Apostolopoulou, M. Vlasiou, P.A. Tziouris, C. Tsiafoulis, A.C. Tsipis, D. Rehder, T.A. Kabanos, A.D. Keramidas, E. Stathatos, Inorg. Chem. 54 (2015) 3979–3988. Doi: 0.1021/acs.inorgchem.5b00159.
[6] D. Rehder, Inorganica Chim. Acta. 455 (2017) 378–389, https://doi.org/10.1016/j.ica.2016.06.021.
[7] D. Rehder, Metallomics. 7 (2015) 730–742, https://doi.org/10.1039/C4MT00304G.
[8] O.J. D'Cruz, Y. Dong, F.M. Uckun, Biochem. Biophys. Res. Commun. 302 (2) (2003) 253–264, https://doi.org/10.1016/S0006-291X(03)00161-X.
[9] A. Ross, D.C. Soares, D. Covelli, C. Pannecouque, L. Budd, A. Collins, N. Robertson, S. Parsons, E. De Clercq, P. Kennepohl, P.J. Sadler, Inorg. Chem. 49 (2010) 1122–1132. Doi: 10.1021/ic9020614.
[10] S.Y. Wong, R.W.Y. Sun, N.P.Y. Chung, C.L. Lin, C.M. Che, Chem. Commun. 28 (2005) 3544–3546, https://doi.org/10.1039/b503535j.
[11] I. Correia, P. Adão, S. Roy, M. Wahba, C. Matos, M.R. Maurya, F. Marques, F.R. Pavan, C.Q. F. Leite, F. Avecilla, J. C. Pessoa, J. Inorg. Biochem. 141(2014)83–93. Doi: 10.1016/j.jinorgbio.2014.07.019.
[12] J.C. Pessoa, S. Etcheverry, D. Gambino, Coord. Chem. Rev. 301–302 (2015) 24–48, https://doi.org/10.1016/j.ccr.2014.12.002.
[13] D. Rehder, Dalton Trans. 42 (2013) 11749–11761, https://doi.org/10.1039/c3dt50457c.
[14] Y. Yoshikawa, H. Sakurai, D.C. Crans, G. Micera, E. Garribba, Dalton Trans. 43 (2014) 6965–6972, https://doi.org/10.1039/C3DT52895B.
[15] S.I. Pillai, S.P. Subramanian, M. Kandaswamy, Eur. J. Med. Chem. 63 (2013) 109–117, https://doi.org/10.1016/j.ejmech.2013.02.002.
[16] M. Sedighipoor, A.H. Kianfar, G. Mohammadnezhad, H. Görls, W. Plass, A.A. Momtazi-Borojeni, E. Abdollahi, Inorganica Chim. Acta. 488 (2019) 182–194. https://doi.org/10.1016/j.ica.2018.12.051.
[17] P. Kalaivani S. Saranya P. Poornima R. Prabhakaran F. Dallemer V. Vijaya Padma K. Natarajan Eur. J. Med. Chem. 82 2014 584 599 10.1016/j.ejmech.2014.05.075.
[18] R. Kurtaran, L. Yildirim, A. Azaz, H. Namli, O. Atakol, J. Inorg. Biochem. 99 (2005) 1937–1944, https://doi.org/10.1016/j.jinorgbio.2005.05.016.
[19] W. Rui, X. Tian, P. Zeng, W. Liu, P. Ying, H. Chen, J. Lu, N. Yang, H. Chen, Polyhedron. 117 (2016) 803–816, https://doi.org/10.1016/j.poly.2016.07.021.
[20] B. Kaya, B. Atasever-Arslan, Z. Kalkan, H. Gür, B. Ülküseven, Gen. Physıol. Bıophys. 35 (2016) 451–458, https://doi.org/10.4149/gpb.2016006a.
[21] B. Atasever, B. Ülküseven, T. Bal-Demirci, S. Erdem-Kuruca, Z. Solakoğlu, Invest New Drugs. 28 (2010) 421–432, https://doi.org/10.1007/s10637-009-9272-2.
[22] Z. Afrasiabi, E. Sinn, W. Lin, Y. Ma, C. Campana, S. Padhye, J. Inorg. Biochem. 99 (2005) 1526–1531, https://doi.org/10.1016/j.jinorgbio.2005.04.012.
[23] Ş. Güveli, J. Coord. Chem. 73 (2020) 137–153, https://doi.org/10.1080/00958972.2020.1711888.
[24] R. Yanardag, T.B. Demirci, B. Ülküseven, S. Bolkent, S. Tunali, S. Bolkent, Eur. J. Med. Chem. 44 (2009) 818–826, https://doi.org/10.1016/j.ejmech.2008.04.023.
[25] L. Ze-hua, D. Chun-ying, L. Ji-hui, L. Yong-jiang, M. Yu-hua, Y. Xiao-zeng, New J. Chem. 2 (2000) 1057–1062, https://doi.org/10.1039/b004846l.
[26] Bruker. APEX2 and SAINT Bruker AXS Inc. 1998.
[27] G. Sheldrick, SHELXL-2014: University of Gottingen and Bruker AXS, Karlsruhe, 2014.
[28] G.M. Sheldrick, SHELXT –Crystallogr A Found Adv. 71 (2015) 3–8. Doi: 10.1107/S2053273314026370.
[29] M.J. Frisch, G.W. Trucks, H.B. Schlegel, G. Scuseria, M. Robb, J. Cheeseman, G. Scalmani, V. Barone, B. Mennucci, G. Petersson, H. Nakatsuji, M. Caricato, H. P.H. X. Li, A.F. Izmaylov, M. Bloino, G. Zheng, J.L. Sonnenberg, M. Hada, M. Ehara, K. Toyota, R. Fukuda, J. Hasegawa, M. Ishida, T. Nakajima, Y. Honda, O. Kitao, H. Nakai, T. Vreven, J.A.M. Jr., J.E. Peralta, F. Ogliaro, J.R. Bearpark, J.J. Heyd, E. Brothers, K.N. Kudin, V.N. Staroverov, R. Kobayashi, Normand, J.E. Rendell, K.A.J. C. Burant, S.S. Iyengar, J. Tomasi, M. Cossi, N. Rega, J.M. Millam, M. Klene, A.J. Knox, J.B. Cross, V. Bakken, C. Adamo, J. Jaramillo, R. Gomperts, R.E. Stratmann, O. Yazyev, G.A. Austin, R. Cammi, C. Pomelli, J.W. Ochterski, R.L. Martin, K. Morokuma, V.G. Zakrzewski, J. Voth, P. Salvador, J.J. Dannenberg, S. Dapprich, A.

D.D.O. Farkas, J.B. Foresman, J.V. Ortiz, W.C. Cioslowski, D.J. Fox, Gaussian 09 Revision A. 02, Gaussian Inc Wallingford CT 200 (2009).
[30] C. Yamazaki, Can. J. Chem. 53 (1975) 610–615, https://doi.org/10.1139/v75-085.
[31] Y. Kurt, B. İlhan-Ceylan, M. Açıkgöz, E. Tüzün, G. Atun, B. Ülküseven, Polyhedron. 65 (2013) 67–72, https://doi.org/10.1016/j.poly.2013.08.010.
[32] R. Apak, K. Güçlü, M. Özyürek, S.E. Karademir, J. Agric. Food Chem. 52 (2004) 7970–7981, https://doi.org/10.1021/jf048741x.
[33] R. Apak, J. Agric. Food Chem. 67 (2019) 9187–9202, https://doi.org/10.1021/acs.jafc.9b03657.
[34] N.V. Gerbeleu, V.B. Arion, J. Burgess, Template synthesis of macrocyclic compounds, Wiley-VCH, Weinheim; New York, 1999.
[35] S. Dekar, K. Ouari, S. Bendia, D. Hannachi, J. Weiss, J. Organomet. Chem. 866 (2018) 165–176, https://doi.org/10.1016/j.jorganchem.2018.04.015.
[36] P. Jeyaraman, A. Alagarraj, R. Natarajan, J. Biomol. Struct. Dyn. 38 (2) (2020) 488–499, https://doi.org/10.1080/07391102.2019.1581090.
[37] A.M. Abu-Dief, L.A.E. Nassr, J. Iran. Chem. Soc. 12 (6) (2015) 943–955, https://doi.org/10.1007/s13738-014-0557-9.
[38] B. İlhan Ceylan, J. Turk. Chem. Soc., Sect. A: Chem. 3 (2016), https://doi.org/10.18596/jotcsa.33245.
[39] A.W. Addison, T.N. Rao, J. Reedijk, J. van Rijn, G.C. Verschoor, J. Chem. Soc. Dalton Trans. (1984) 1349–1356, https://doi.org/10.1039/DT9840001349.
[40] V.M. Leovac, V. Dıvjakovıc, V.I. Cesljevıs, Polyhedron 6 (10) (1987) 1901–1907, https://doi.org/10.1016/S0277-5387(00)81101-8.
[41] İ. Gönül, Inorganica Chim. Acta 495 (2019) 119027–119034, https://doi.org/10.1016/j.ica.2019.119027.
[42] Ş. Güveli, N. Özdemir, T. Bal-Demirci, M.S. Soylu, B. Ülküseven, Transit. Met. Chem. 44 (2019) 115–123, https://doi.org/10.1007/s11243-018-0275-8.
[43] L.M. Fostiak, I. Garcia, J.K. Swearingen, E. Bermejo, A. Castineiras, D.X. West, Polyhedron 22 (2003) 83–92, https://doi.org/10.1016/S0277-5387(02)01330-X.
[44] B. İlhan-Ceylan, E. Tuzun, Y. Kurt, M. Acikgoz, S. Kahraman, G. Atun, B. Ulkuseven, J. Sulfur Chem. 36 (2015) 434–449, https://doi.org/10.1080/17415993.2015.1050396.
[45] M. Vlasiou, C. Drouza, T.A. Kabanos, A.D. Keramidas, J. Inorg. Biochem. 147 (2015) 39–43, https://doi.org/10.1016/j.jinorgbio.2015.01.010.
[46] Y. Kurt, N.G. Deniz, J. Coord. Chem. 68 (2015) 4070–4081, https://doi.org/10.1080/00958972.2015.1086760.
[47] Y. Kurt, A. Koca, M. Akkurt, B. Ülküseven, Inorganica Chim. Acta. 388 (2012) 148–156, https://doi.org/10.1016/j.ica.2012.03.023.
[48] P.E. Aranha, J.M. Souza, S. Romera, L.A. Ramos, M.P. dos Santos, E.R. Dockal, E.T. G. Cavalheiro, Thermochim. Acta. 453 (2007) 9–13, https://doi.org/10.1016/j.tca.2006.11.001.
[49] B. İlhan-Ceylan, A. Yilmaz, O. Bölükbaşı, E. Türker-Acar, M. Özyürek, Y. Kurt, B. Ülküseven, J. Coord. Chem. 73 (1) (2020) 120–36. Doi: 10.1080/00958972.2020.1715372.
[50] S. Rayati, N. Torabi, A. Ghaemi, S. Mohebbi, A. Wojtczak, A. Kozakiewicz, Inorganica Chim. Acta. 361 (2008) 1239–1245, https://doi.org/10.1016/j.ica.2007.08.004.
[51] P.A. Saswati, S. Majumder, S.P. Dash, S. Roy, M.L. Kuznetsov, J. C. Pessoa, C. S. B. Gomes, M. R. Hardikar, E.R.T. Tiekink, R. Dinda, Dalt Trans. 47(33) (2018) 11358-11374. Doi: 10.1039/C8DT01668B.
[52] P. Galloni, V. Conte, B. Floris, Coord. Chem. Rev. 301–302 (2015) 240–299, https://doi.org/10.1016/j.ccr.2015.02.022.
[53] S.A. Hosseini-Yazdi, S. Hosseinpour, A. Akbar Khandar, W. Scott Kassel, N.A. Piro, Inorganica Chim. Acta. 427 (2015) 124–130, https://doi.org/10.1016/j.ica.2014.12.011.
[54] S.A. Hosseini-Yazdi, P. Samadzadeh-Aghdam, R. Ghadari, Polyhedron 160 (2019) 35–41, https://doi.org/10.1016/j.poly.2018.12.019.
[55] N. Arshad, M. Ikramullah, M Sher Aamir, Monatsh. Chem. 148 (2017) 245–255, https://doi.org/10.1007/s00706-016-1768-9.
[56] S. Krapf, Zur Theorie des Ladungstransfers in Biopolymeren: von der Thermodynamischen Integration zu angeregten Zuständen (Dissertation) - Contributions to the Charge Transfer Theory in Biopolymers: from Thermodynamic Integration to Excited States (PhD Thesis in German). https://doi.org/10.13140/RG.2.1.2679.7286 (2015).
[57] M. Martínez-Cifuentes, R. Salazar, O. Ramírez-Rodríguez, B. Weiss-López, R. Araya-Maturana, Molecules, 22 (2017) 577–587. Doi: 10.3390/molecules22040577.
[58] J. Sochor, J. Dobes, O. Krystofova, B. Ruttkay-Nedecky, P. Babula, M. Pohanka, T. Jurikova, O. Zitka, V. Adam, B. Klejdus, R. Kizek, Int. J. Electrochem. Sci., 8 (2013) 8464–8489.
[59] M. Asadi, Z. Asadi, N. Savaripoor, M. Dusek, V. Eigner, M.R. Shorkaei, M. Sedaghat, Spectrochim. Acta A 136 (2015) 625–634, https://doi.org/10.1016/j.saa.2014.09.076.
[60] A.M. Abu-Dief, L.H. Abdel-Rahman, A.A.H. Abdel-Mawgoud, Appl. Organomet. Chem. 34 (2020) 1–20, https://doi.org/10.1002/aoc.5373.
[61] E. Bagdatli, E. Altuntas, U. Sayin, J Mol Struct. 1127 (2017) 653–661, https://doi.org/10.1016/j.molstruc.2016.08.026.
[62] I. Belkhettab, S. Boutamine, H. Slaouti, M.F. Zid, H. Boughzala, Z. Hank, J. Mol. Struct. 1206 (2020), https://doi.org/10.1016/j.molstruc.2019.127597.
[63] S.R. Maxwell, Drugs. 49 (1995) 345–436, https://doi.org/10.2165/00003495-199549030-00003.
[64] İ. Gönül, M. Köse, G. Ceyhan, S. Serin, Inorganica Chim. Acta. 453 (2016) 522–530, https://doi.org/10.1016/j.ica.2016.09.004.
[65] S.N. Kertmen, İ. Gönül, M. Köse, J. Mol. Struct. 1152 (2018) 29–36, https://doi.org/10.1016/j.molstruc.2017.09.067.
[66] B. Halliwell, J.M. Gutteridge, Biochem J. 219 (1984) 1–14, https://doi.org/10.1042/bj2190001.
[67] A.M. Sarhan, S.A. Elsayed, M.M. Mashaly, A.M. El-Hendawy, Appl Organometal. Chem. 33 (2019) 1–16, https://doi.org/10.1002/aoc.4655.